Direct numerical simulation of oxide inclusion turbulent deposition at liquid steel/slag interface

Arunvady Xayasenh, Magali Dupuy, Laurent Joly, Hervé Duval

Direct numerical simulation of oxide inclusion turbulent deposition at liquid steel/slag interface

Arunvady Xayasenh[1], Magali Dupuy[1], Laurent Joly[2], Hervé Duval[1]

[1] *Laboratory of Chemical Engineering and Materials, École Centrale Paris, Châtenay-Malabry, France*
[3]*Aerodynamic, Energetic and Propulsion Department, Institut Supérieur de l'Aéronautique et de l'Espace, Toulouse, France*

Keywords: direct numerical simulation, Lagrangian particle tracking, turbulent deposition, free-slip interface

Abstract

The present study focuses on the inclusion behaviour near the liquid metal/slag interface. Inclusion turbulent deposition is investigated using direct numerical simulation of the liquid flow combined with Lagrangian particle tracking under conditions of one-way coupling. The interface is modelled as a non-deformable free-slip surface. Unsheared turbulence is generated by random forcing in a finite-height region parallel to the free-slip surface. In between, the turbulence diffuses toward the free surface. The inclusions are randomly introduced in the forcing region and tracked through the diffusion region up to the interface. In the particle dynamic equation, the buoyancy force, the Stokes drag, the pressure drag and the added mass are considered. Close to the interface, the hydrodynamic interactions (i.e. lubrication effects) between the inclusion and the free surface may be taken into account as well as the Van der Waals forces.
Numerical simulations were performed with surface Reynolds numbers Re_S ranging from 68 to 235. The inclusion diameter varied between 10^{-5}m and 5.10^{-5}m and the particle to liquid density ratio between 0.5 and 1. For these sets of parameters, it appears that the inertia effects are very weak. The deposition of buoyant inclusions is controlled by sedimentation whereas for nonbuoyant inclusions, direct interception is the only deposition mechanism. In the latter case, the deposition velocity strongly depends on Re_S. It is shown that the deposition velocity made dimensionless by the free surface characteristic velocity scales as the inclusion diameter made dimensionless by the Kolmogorov length scale calculated at the free surface. Lastly, the effect of lubrication is examined: it can significantly reduce the direct interception contribution of the deposition velocity.

Introduction

For the steelmaking industry, mastering the inclusion content represents a key point since both the quality of the products and the lifetime of the processing tools are related to it. Inclusions are solid particles (often made of metallic oxides) of micrometer to millimeter size, dispersed in the metallic phase. The so-called vacuum ladle treatment of liquid metal is the processing stage mainly responsible for the inclusion concentration of the specialty steels. In this process, inclusions are transported by the turbulent liquid metal flow from the bulk to the interface between the liquid metal and a second non-miscible liquid phase, where inclusions are captured. This second phase called slag (which covers the liquid metal to be refined) is a mixture of metallic oxides.
The first numerical simulations of liquid steel ladle were performed in the late 1970s (Szekely et al. 1979). With the increase of the computational capability, more advanced and complex numerical models were developed. Process simulations using k-ε models in order to solve the flow field in the ladle have been run by Miki et al. (1997) or Shang et al. (2002). Numerous ladle simulations were conducted under the leadership of KTH in Stockholm (Hallberg et al. 2005) and the University of Urbana-Champaign (Aoki et al. 2004). A thorough presentation of the different modelling approaches can be found in Zhang (2006).
The latter numerical simulations should be regarded as macroscopic models of processes where the behaviour and the capture of inclusions at interfaces is not yet accurately described, in particular, at the liquid steel/slag interface (De Felice et al. 2012). The present study tries to bridge this gap and focuses on the turbulent transport (and subsequent capture) of the inclusions in the vicinity of the liquid metal/slag interface. This study also comes in addition to the research on transport and deposition of particles in hydrosol since most publications are related to aerosol (Brooke et al. 1994, Narayanan et al. 2003, Tian & Ahmadi 2007, Gao et al. 2012). On top of that, deposition on solid walls has been widely examined (Wood 1981, Fan & Ahmadi 1993, Guha 1997, Lai 2005, Zhao & Wu 2006) while deposition on a free surface such as a liquid steel/slag interface is not so extensively dealt with (Van Haarlem et al. 1998, De Felice et al. 2012).
In the following, we start with the description of the particle deposition numerical model. Then, the model is applied to the deposition of hypothetic non-buoyant inclusions and to the deposition of real buoyant alumina inclusions at liquid steel/slag interface. The main purposes of this paper are (i) to identify and to quantify the deposition mechanisms, (ii) to establish the suitable kinetic laws for inclusion turbulent deposition.

Nomenclature

C	particle concentration (m^{-3})
d_p	particle diameter (m)
f	friction coefficient
g	gravitational constant ($m.s^{-2}$)
H	Hamaker constant (J)
J	particle mass transfer rate ($m^{-2}.s^{-1}$)
k	turbulent kinetic energy ($m^2.s^{-2}$)
l_s	surface Kolmogorov length scale (m)
L	domain length (m)
$\boldsymbol{n}$	unit vector normal to the interface
N	number of grid points
Re	Reynolds number
t	time (s)
u	velocity ($m.s^{-1}$)
u_d	deposition velocity ($m.s^{-1}$)
x, y, z	space coordinates (m)

Greek letters

δ^+	reduced separation distance
ε	dissipation rate ($m^2.s^{-3}$)
μ	dynamic viscosity (Pa.s)
ν	kinematic viscosity ($m^2.s^{-1}$)
ρ	density ($kg.m^{-3}$)

Subscripts

d	deposition
f	fluid
p	particle
s	surface
$\parallel$	parallel to the interface
$\perp$	perpendicular to the interface

Superscripts

‘	fluctuation

Numerical Model

The present model describes the inclusion transport in a thin layer adjacent to the liquid metal/slag interface. It combines direct numerical simulation (DNS) of the liquid metal flow together with Lagrangian tracking of the inclusions under conditions of one-way coupling. In our approach, the turbulence is generated away from the interface and diffuses towards it. It is also assumed that the mean velocity of the liquid metal in the vicinity of the interface is negligible. Furthermore, the interface is modeled as a non-deformable free-slip surface.

Liquid metal turbulent flow

The turbulent flow field is obtained using the DNS solver developed by Campagne (2006). It solves the Navier-Stokes equations considered for an incompressible fluid.
The space discretization is based on a pseudospectral method: the linear terms are evaluated in the spectral space and the nonlinear terms are evaluated in the physical space (Campagne et al 2009). A third-order Runge-Kutta scheme is used for advancement of the convective terms while a second-order Crank-Nicholson scheme is used for the viscous terms. The resulting discretization scheme is second-order accurate in time.
The governing equations are solved on a rectangular domain of dimensions L_x, L_y, L_z, with L_z the vertical dimension. This domain is divided in three regions as represented in figure 1. The first region is located in the middle of the domain between the top and bottom boundaries and is of $L_z/3$ height. It corresponds to the region where the turbulence is produced thanks to Alvélius method (Alvélius 1999) which generates a random, zero-mean, three-dimensional, and isotropic turbulent force field in the spectral space. This turbulence production region feeds two neighbouring ones where turbulence is diffused towards the top and bottom horizontal boundaries, respectively.

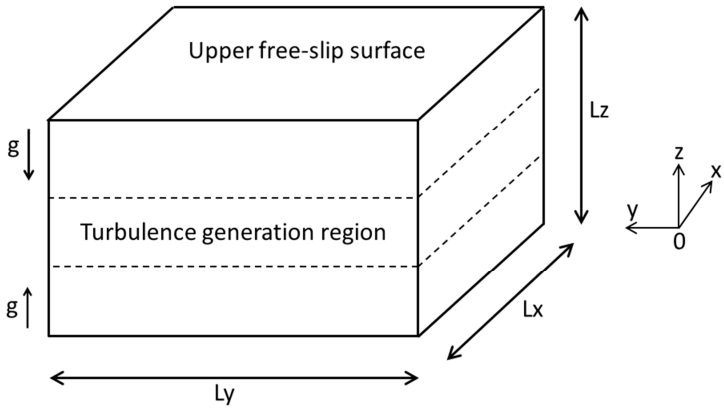

Figure 1: Representation of the computational domain.

The flow is assumed to be periodic in the horizontal directions, with periods L_x and L_y. At the $z = 0$ and $z = L_z$ boundaries, impermeability and free-slip conditions are imposed.

Inclusion trajectory

When a statistically steady flow field is reached, inclusions are randomly introduced in the turbulence generation region. They are transported towards the horizontal surfaces by the turbulent flow field. It is assumed that once a particle touches the free surface, the deposition process is completed with no rebound effects included. For every inclusion deposited, another is added in the turbulence generation region in order to maintain a constant particle number in the computational domain.

Lagrangian particle tracking is considered. Particle effects on flow as well as particle-particle interaction are not taken into account. The particle equation of motion is given as

$$\frac{1}{6}\pi\rho_p d_p^3\frac{d\boldsymbol{u}_p}{dt} = -3\pi\mu_f d_p(\boldsymbol{u}_p-\boldsymbol{u}_f)+\frac{1}{6}\pi d_p^3(\rho_p-\rho_f)\boldsymbol{g} + \frac{1}{12}\pi\rho_f d_p^3\left(\frac{D\boldsymbol{u}_f}{Dt}-\frac{d\boldsymbol{u}_p}{dt}\right) + \frac{1}{6}\pi\rho_f d_p^3\frac{D\boldsymbol{u}_f}{Dt} \quad (1)$$

where d_p is the particle diameter, μ_f the dynamic fluid viscosity, and ρ_p and ρ_f are, respectively, the particle density and the fluid density. Here $\boldsymbol{g}$ denotes the acceleration of gravity which is opposite to the closest free-slip surface (figure 1), $\boldsymbol{u}_p$ is the particle velocity and $\boldsymbol{u}_f$ is the fluid velocity in the absence of the particle. This local undisturbed fluid velocity $\boldsymbol{u}_f$ is evaluated at the particle center using Hermite interpolation in the three space directions. $D\boldsymbol{u}_f/Dt = \partial\boldsymbol{u}_f/\partial t + \boldsymbol{u}_f.\nabla\boldsymbol{u}_f$ is the fluid acceleration at the instantaneous particle center. d/dt corresponds to the time derivative following the moving inclusion.

In Eq. (1), the left-hand side represents the particle inertial force. On the right-hand side, the terms are the Stokes drag force (since the Reynolds particle number $Re_p = \rho_f\|\boldsymbol{u}_p-\boldsymbol{u}_f\|(d_p/2)/\mu_f$ is much lower than 1), the gravitational force, the added-mass force and the effects of pressure gradient of the undisturbed flow. In Eq. (1), the lift force, the Faxen corrections close to the surface as well as the Basset history term are neglected. Brownian diffusion is neglected since particle diameter is much larger than 1 µm.

When the particle is close to the free surface (i.e., when the distance δ between the center of the particle and the interface is lower than about $20\ d_p$), it is possible to include the hydrodynamic interactions between the particle and the interface (i.e. lubrication effects) in the particle equation of motion. The lubrication effects are taken into account through the introduction of the appropriate friction coefficients (Nguyen & Evans 2002, Nguyen & Evans 2004, Nguyen & Jameson 2005) in the Stokes steady drag:

$$F_{D\parallel} = -3\pi\mu_f d_p\left(f_{\parallel,1}u_{p,\parallel}-f_{\parallel,2}u_{f,\parallel}\right)$$
$$F_{D\perp} = -3\pi\mu_f d_p\left(f_{\perp,1}u_{p,\perp}-f_{\perp,2}u_{f,\perp}\right) \quad (2)$$

where the subscript $\perp$ (resp. $\parallel$) is associated with the component perpendicular (resp. parallel) to the interface. The friction coefficients essentially depend on the reduced separation distance $\delta^+ = 2\delta/d_p - 1$. It should be noted that the friction coefficient $f_{\perp,1}$ acting on the perpendicular component of the particle velocity, diverges as the reduced separation distance vanishes. When lubrication effects are incorporated in the particle equation of motion, the (attractive) Van Der Waals interactions between the particle and the slag close to the free surface are included as well:

$$\boldsymbol{F}_{VdW} = \alpha_r\frac{4}{3}\frac{(H/d_p)}{\delta^{+2}(\delta^+ + 2)^2}\boldsymbol{n} \quad (3)$$

where H is the so-called Hamaker constant ($H = 10^{-19}$ J for alumina/liquid iron/alumina configuration), which depends on the inclusion, slag and liquid metal nature, α_r is the retardation coefficient of the London interaction energy and $\boldsymbol{n}$ is a unit vector normal to the interface and directed outwardly (with respect to the liquid metal). The drainage of the liquid film separating the inclusion from the slag phase is achieved thanks to the Van der Waals attraction.

The particle equation of motion (1) is solved numerically using third-order Adams-Bashforth method.

The deposition velocity u_d is defined as

$$u_d = \frac{J}{C} \quad (4)$$

where J is the particle mass transfer rate and C the mean particle concentration. Some authors prefer to define the deposition velocity as the particle mass transfer rate to bulk particle concentration ratio (Hussein et al. 2012, Sippola & Nazaroff 2004). But, as noted by Guha (1997), mean concentration can be used instead of the bulk one, as done by Van Haarlem et al. (1998). In our case, it turns out that the mean and bulk concentrations are almost equal because the particle concentration remains constant in the domain height but for a small region close to the interface (see figure 3 in the next section).

Results and Discussion

Simulation parameters

As the Alvélius method (Alvélius 1999) creates a zero-mean turbulence field, the entire flow is characterised by the generated velocity fluctuations of the turbulence motion. Thus, the velocity fluctuations $\boldsymbol{u}'$correspond to the fluid velocity, that is to say $\boldsymbol{u}' = \boldsymbol{u}_f$. Another consequence of the zero-mean turbulence field is that the deposition of inclusions directly depends on the flow fluctuations behaviour towards the free-surface. This behaviour can be explicitly related to the surface values of the turbulent kinetic energy k_s and dissipation rate ε_s (Campagne 2009). Therefore, the different simulation configurations possible in this study are controlled by the value of the surface Reynolds number $Re_S = k_s^2/(\nu_f\varepsilon_s)$.

In DNS, the number of grid points N necessary to solve all the turbulence scales depends on the Reynolds number as (Comte-Bellot & Bailly 2003)

$$N \propto Re^{9/4} \quad (5)$$

In other words, the required spatial resolution grows rapidly with the target Reynolds number, here found at the boundary of the forcing region. Besides, as mentioned by Campagne (2006), since the local Reynolds number decreases in the pure self-diffusion region towards the free-slip surface, for a given Reynolds number at the forcing region boundary, the surface Reynolds number also depends on the distance at which the free-slip surface is placed: the closer the free-slip surface, the higher the surface Reynolds number.

In this study, different values of $N_x \times N_y \times N_z$ grid are investigated on two different domain sizes $L_x \times L_y \times L_z$, with the corresponding Reynolds number Re_S as given in table 1.

$L_x = L_y$ (cm)	5.4	5.4	5.4	5.4
L_z (cm)	4.7	3.1	4.7	4.7
$N_x = N_y$	192	192	288	384
N_z	168	112	252	336
Re_S	68	103	148	235

Table 1: Domain size and number of grid points in the x, y, z directions considered for the simulations and associated surface Reynolds number Re_S.

Particle trajectories are computed for different sets of parameters, with the particle diameter varying between 10^{-5}m and 5.10^{-5}m and the particle to liquid density ratio varying between 0.5 (alumina inclusions) and 1 (hypothetic non-buoyant inclusions). The properties of the inclusions and of the liquid metal are summarized in table 2. Some simulations are performed without inertia effects (resp. gravity): in this case, particle inertial force, added mass force and pressure gradient force (resp. gravitational force) are removed from Eq. (1).
The number of particles introduced in the computational domain is arbitrary chosen equal to 20000 (for each set of parameters).

d_p (μm)	ρ_p $(kg.m^{-3})$	ρ_f $(kg.m^{-3})$	ν_f $(m^2.s^{-1})$
10 to 50	3500 to 7000	7000	7.85×10^{-7}

Table 2: Inclusion and liquid metal characteristics.

Liquid turbulent flow

We briefly report hereafter some results (Campagne 2006, Campagne et al. 2009) in connection with our problem. Close to the free-slip surface, the flow field is structured in three different layers. An outer layer called the “blockage” layer matches the region where the velocity anisotropy starts to decrease, going from the equilibrium value of the turbulence diffusion region to zero at the surface, as pictured in figure 2. The blockage layer is a consequence of the impermeability condition. Another layer, called the “slip” layer, is due to the free-slip condition and is defined as region across which the tangential vorticity fluctuation decreases down to zero at the surface. The third layer is located in the immediate vicinity of the surface and corresponds to the Kolmogorov layer introduced by Brumley & Jirka (1988) and Calmet & Magnaudet (2003). According to these authors, the normal root mean square velocity fluctuation follows its asymptotic linear behaviour all across this region.

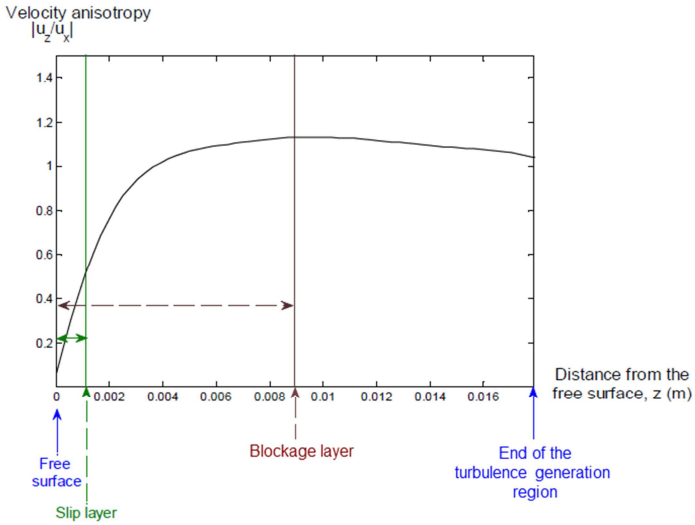

Figure 2: Evolution of the velocity anisotropy versus the distance from the free surface and designation of the different layers in the diffusion region. ($Re_S = 68$).

In figure 3, the evolution in the domain height of the tangential and normal fluid velocities is depicted. It can be seen that at the interface, the normal fluid velocity is equal to zero whereas the tangential fluid velocity is not, which is a characteristic of free-surfaces.

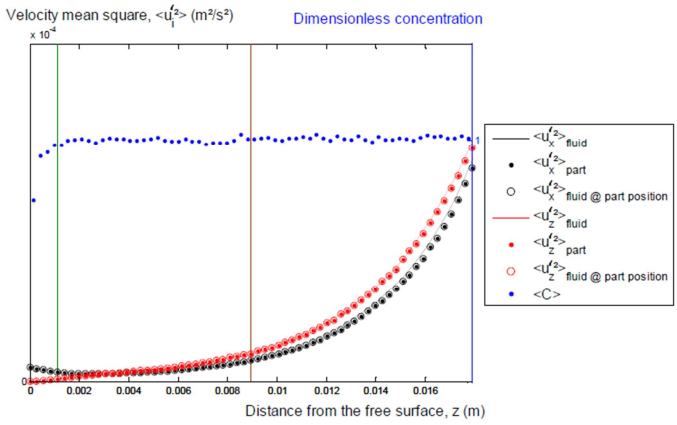

Figure 3: Evolution of fluid velocity and particle concentration in the diffusion layer. ($Re_S = 68$).

Inclusion deposition

Figure 4 shows the variations of the particle deposition velocity as a function of the particle diameter when inertia effects are taken into account and when they are neglected. The simulations were performed for two values of the surface Reynolds number, i.e. $Re_S = 68$ and $Re_S = 235$, and two values of the particle to liquid density ratio, i.e. $\rho_p/\rho_f = 1$ and $\rho_p/\rho_f = 0.5$, respectively. The simulations were run without gravity since gravitational effect might be of great influence on particle deposition and hide the effects of inertia. Figure 4 shows that the difference in deposition velocity, depending on whether inertia effects are included or not, remains small. We think that inertial effects are presently not significant on deposition and that the velocity difference is essentially a consequence of the computational approximations. The negligible role of inertia is confirmed

in figure 3 which shows the variations of the root mean square velocity fluctuation of the fluid, as well as of the fluid at the position of the particles and of the particles themselves: it reveals that the particle fluctuations follow the fluid fluctuations. Thus it can be concluded that for non-buoyant inclusions direct interception is the main deposition mechanism (inclusion deposition by direct interception occurs specifically because inclusions are finite in size: considering inclusions moving along liquid metal streamlines, any inclusion will be deposited that comes within one inclusion's radius from the interface). Figure 4 also points out that the efficiency of the direct interception mechanism strongly depends on the surface Reynolds number Re_S.

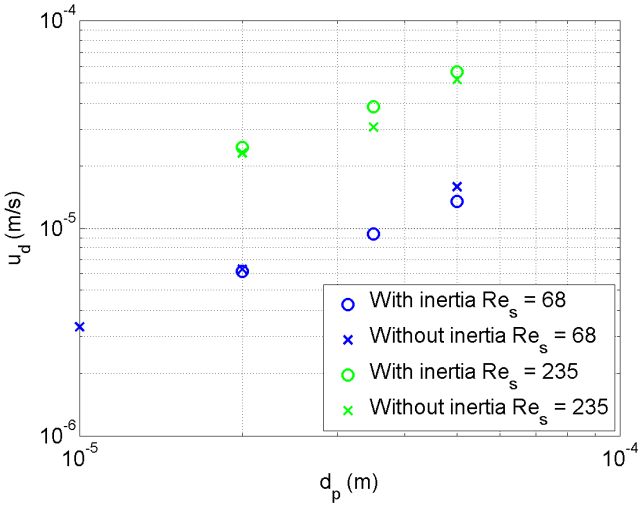

Figure 4: Effects of inertial effects on the deposition velocity for different surface Reynolds number Re_S (simulations without gravity). (When $Re_S = 68, \rho_p/\rho_f = 1$ and when $Re_S = 235, \rho_p/\rho_f = 0.5$).

This effect is examined in details in figure 5 which presents the variations of the dimensionless deposition velocity as a function of the dimensionless particle diameter for simulations where neither gravity nor inertia effects have been taken into account. The deposition velocity and the particle diameter are made dimensionless using the characteristic surface velocity u_s and the characteristic Kolmogorov surface length scale l_s respectively defined as

$$u_s = \left(\nu_f \varepsilon_s\right)^{1/4} \tag{6}$$

$$l_s = \frac{\nu_f^{3/4}}{\varepsilon_s^{1/4}} \tag{7}$$

Figure 5 suggests that the dimensionless deposition velocity evolves as a linear function of the dimensionless particle diameter. The data are actually well fitted by the following law:

$$\frac{u_d}{u_s} = A_1 \left(\frac{d_p}{l_s}\right) \tag{8}$$

where $A_1 = 0.097$.

This scaling concords with Brooke et al. (1994) and Campagne et al. (2009) findings. Indeed, as explained by Brooke et al. (1994), the deposition velocities due to turbulent diffusion should be of the order of the root mean square of the fluid velocity fluctuations estimated at the distance $d_p/2$ of the deposition surface, i.e.,

$$u_d \sim rms\left[u_z'(z = \frac{d_p}{2})\right] \tag{9}$$

Besides, Campagne et al. (2009) found that the normal rms fluctuations follow an asymptotic linear behavior all across the Kolmogorov layer adjacent to the free surface. Specifically, they found that:

$$\frac{rms[u_z']}{u_s} = A_2 \frac{z}{l_s} \tag{10}$$

where $A_2 = 0.62$. As far as inclusion deposition is concerned, the value of the normal rms fluctuations has to be estimated at the location $z = \frac{d_p}{2}$. As a consequence, Eq. (10) can be compared with Eq. (8) where A_1 corresponds to $A_2/2$. It should be noted that the discrepancy between the two constants A_1 and $A_2/2$ is due to the fact that only the normal velocity fluctuations directed towards the interface can lead to a deposition process. Furthermore, Campagne (2006) and Bodard (2009) noticed a strong dissymmetry between impact and ejection events in the vicinity of the free surface: the impacts of fluid at the free surface are less frequent (but more energetic) than the ejections events.

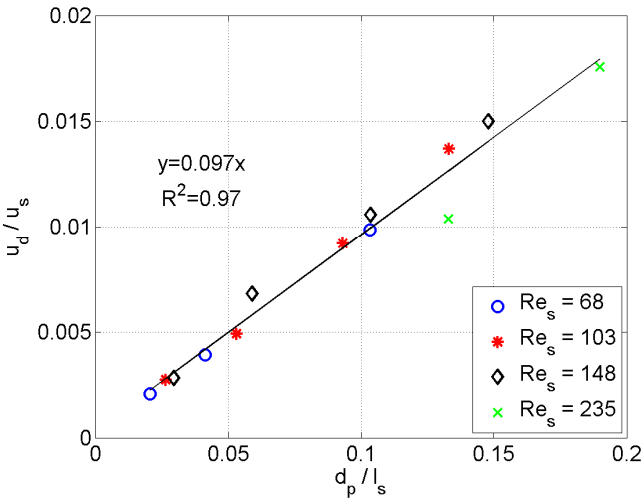

Figure 5: Evolution of dimensionless deposition velocity versus dimensionless particle diameter for simulations run without gravity and inertial effects and for different surface Reynolds number Re_S.

The effects of lubrication have also been investigated for simulations run without gravity or inertia effects. Results are plotted in figure 6 where the dimensionless deposition velocity obtained with or without lubrication is depicted for different values of the surface Reynolds number Re_S. It can be observed that for non-buoyant inclusions, lubrication significantly reduces direct interception, with reductions varying from 40% to 55%.

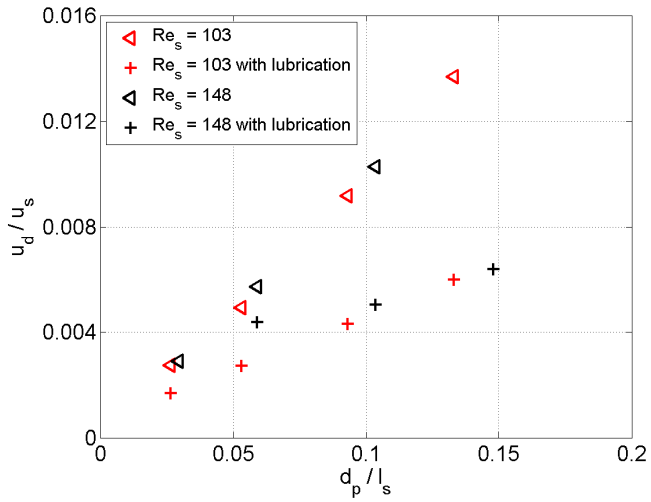

Figure 6: Lubrication effects on dimensionless deposition velocity for simulations run without gravity or inertial effects and for different surface Reynolds Re_S.

Configurations for which gravity is taken into account are investigated in figure 7 for different values of surface Reynolds number Re_S varying between 68 and 235. Unlike for non-buoyant inclusions, figure 7 shows that deposition velocity of buoyant inclusions seems independent of the variations of Re_S, revealing that direct interception has a negligible effect. In figure 7, lubrication is taken into account for an intermediate value of surface Reynolds number Re_S equal to 103. It can be seen that lubrication effects are sensible but remains weak. All simulations depicted in figure 7 give a deposition velocity quasi-identical to the sedimentation velocity indicating that the deposition of alumina inclusions dispersed in liquid steel is controlled by sedimentation for this range of surface Reynolds number Re_S.

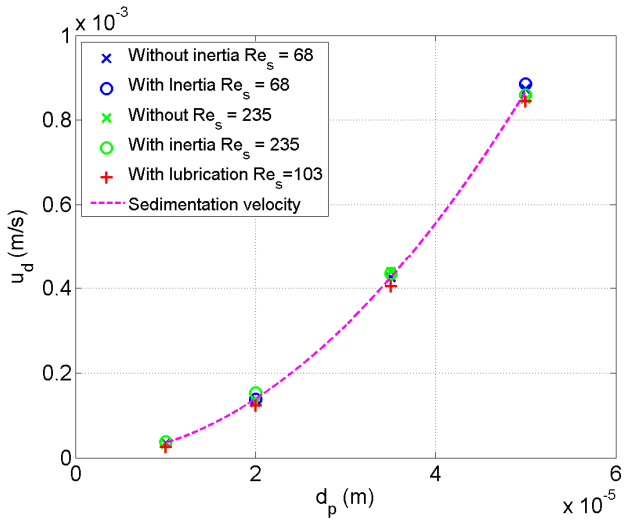

Figure 7: Effects of surface Reynolds number Re_S and lubrication on the deposition velocity for simulations run with gravitational force. ($\rho_p/\rho_f = 0.5$).

In industry, surface Reynolds number can reach higher values than those investigated in this study. Typically, in steelmaking industry, Re_S values vary between 10^3 and 10^7. For such surface Reynolds numbers and considering the law established in Eq. (8), the contribution of direct interception mechanism to deposition velocity can be as great as $7 \times 10^{-4} m/s$ for a particle diameter of $10\mu m$, while the sedimentation velocity is only of $3.5 \times 10^{-5} m/s$ for such inclusions. Thus the contribution of direct interception and sedimentation mechanisms can be differently balanced according to the range of surface Reynolds number considered.

Conclusions

Particle deposition onto a non-deformable free-slip surface has been investigated using direct numerical simulation of the liquid flow combined with Lagrangian particle tracking under conditions of one-way coupling. The inertia and lubrication effects have been studied for buoyant as well as for non-buoyant inclusions.

For non-buoyant inclusions, it has been shown that inertial effects are not significant and that the deposition is mainly due to direct interception, at least in the range of surface Reynolds number investigated (from 68 to 235). Specifically, we have found that the dimensionless deposition velocity scales linearly with the dimensionless particle diameter (made dimensionless thanks to the characteristic scales at the free surface). Besides, the lubrication effects significantly reduce the deposition velocity (about half of the value without hydrodynamic retardation). It should be noted that the case of non-buoyant inclusions studied here might not be relevant of steelmaking industry, where $\rho_p \lesssim \rho_f/2$ for most inclusions, but they are representative of other sectors of the metallurgy industry, such as liquid aluminum processing, for which $\rho_p \approx \rho_f$.

For buoyant inclusions (which characteristics in the present study correspond to steelmaking industry) and for the range of surface Reynolds number investigated (from 68 to 235), deposition is controlled by sedimentation. Inertia and direct interception contributions remain negligible. Besides, lubrication effects, even though sensible, are weak.

However, for greater values of the surface Reynolds number, such as the values encountered in an industrial ladle for instance, we expect that the direct interception contribution to the deposition velocity might be of greater importance than the sedimentation contribution (up to one order of magnitude).

Acknowledgements

This research was supported by the Agence Nationale de la Recherche, as part of the CIREM project (Comportement des Inclusions dans les REacteurs Métallurgiques, project No. ANR06 MATPRO 0005).

References

Alvélius, K. Random forcing of three-dimensional homogeneous turbulence. Physics of Fluids, Vol. 11, 1880-1889 (1999)

Aoki, J. & Thomas, B.G. & Peter, J. & Peaslee, K.D. Proc. of Iron and Steel Technology Conf., AISTech, Warrendale, PA, p.1045 (2004)

Arcen, B. Etude par simulation numérique directe du comportement et de la dispersion de particules en écoulement non homogène isotherme ou anisotherme. PhD thesis, Laboratoire d'Energétique et de Mécanique Théorique Appliquée, Groupe ESSTIN, Vandoeuvre-lès-Nancy (2006)

Bodart, J. Effet de blocage dans un écoulement turbulent non cisaillé. PhD thesis, Institut National Polytechnique de Toulouse (2009)

Brumley, B.H. & Jirka, G.H. Air-water transfer of slightly soluble gases: Turbulence, interfacial processes and conceptual models. PhysicoChem. Hydrodyn., Vol. 10, (1988)

Brooke, J.W. & Hanratty, T. & McLaughlin, J.B. Free-flight mixing and deposition of aerosols. Physics of Fluids, Vol. 6 (1994)

Calmet, I. & Magnaudet, J. Statistical structure of high-Reynolds-number turbulence close to the free surface on an open-channel flow. Journal of Fluid Mechanics, Vol. 474 (2003)

Campagne, G. Simulation numérique directe de l'interaction turbulence/surface libre pour l'analyse du transfert intercomposantes. PhD thesis, Institut national Polytechnique de Toulouse (2006)

Campagne, G. & Cazalbou, J.B. & Joly, L. & Chassaing, P. The structure of a statistically steady turbulent boundary layer near a free-slip surface. Physics of Fluids, Vol. 21 (2009)

Comte-Bellot, G. & Bailly, C. Turbulence, CNRS Éditions (2003)

De Felice, V. & Daoud, I.L.A., Dussoubs, B. & Jardy, A. & Bellot, J.P. Numerical modelling of inclusion behaviour in a gas-stirred ladle. ISIJ International, Vol. 52, No. 7, 1273-1280 (2012)

Fan, F.G. & Ahmadi, G. A sublayer model for turbulent deposition of particles in vertical ducts with smooth and rough surfaces. Journal of Aerosol Science, Vol. 24, No. 1, 45-64 (1993)

Gao, N. & Niu, J. & He, Q. & Zhu, T. & Wu, J. Using RANS turbulence models and Lagrangian approach to predict particle deposition in turbulent channel flows. Building and Environment, Vol. 48, 206-214 (2012)

Guha, A. A unified eulerian theory of turbulent deposition to smooth and rough surfaces. Journal of Aerosol Science, Vol. 28, No. 8, 1517-1537 (1997)

Hallberg, M. & Jönsson, P.G. & Jonsson, T.L.I. & Erikson, R. Process model of inclusion separation in a stirred steel ladle. Scandinavian Journal of Metallurgy, Vol. 34, 41-56 (2005)

Hussein, T. & Smolik, J. & Kerminen, V.M. & Kulmala M. Modeling dry deposition of aerosol particles onto rough surfaces. Aerosol Science and Technology, Vol. 46, 44-59 (2012)

Lai, A.C.K. Modeling indoor coarse particle deposition onto smooth and rough vertical surfaces. Atmospheric Environment, Vol. 39, 3823-3830 (2005)

Miki, Y. & Thomas, B.G. & Denissov, A. & Shimada, Y. Model of inclusion removal during RH degassing of steel. Iron & Steemaker, Vol. 24, No. 8, 31-38 (1997)

Narayanan, C. & Lakehal, D. & Botto, L. & Soldati, A. Mechanisms of particle deposition in a fully developed turbulent open channel flow. Physics of Fluids, Vol. 15, No. 3, 763-775 (2003)

Nguyen, A.V. & Evans, G.M. Axisymmetric approach of a solid sphere toward a non-deformable planar slip interface in the normal stagnation flow – Development of global rational approximations for resistance coefficients. International Journal of Multiphase Flow, Vol. 28, 1369-1380 (2002).

Nguyen, A.V. & Evans, G.M. Exact and global rational approximate expressions for resistance coefficients for a colloidal solid sphere moving in a quiescent liquid parallel to a slip gas-liquid interface. Journal of Colloid and Interface Science, Vol. 273, 262-270 (2004).

Nguyen, A.V. & Jameson, G.J. Sliding of fine particles on the slip surface of rising gas bubbles: resistance of liquid shear flows. International Journal of Multiphase Flow, Vol. 31, 492-513 (2005).

Shang, D. & Söder, M. & Jönsson, P. & Jonsson, L. Modelling micro-inclusion growth and separation in gas-stirred ladles. Scandinavian Journal of Metallurgy, Vol. 31, 134-147 (2002)

Sippola, M.R. & Nazaroff, W.W. Experiments measuring particle deposition from fully developed turbulent flow in ventilation ducts. Aerosol Science and Technology, Vol. 38, 914-925 (2004)

Szekely, J. & Lehner, T. & Chang, C.W. Ironmaking Steelmaking, Vol. 6, p.285 (1979)

Tian, L. & Ahmadi, G. Particle deposition in turbulent duct flows – comparisons of different model predictions. Journal of Aerosol Science, Vol. 38, 377-397 (2007)

Van Haarlem, B. & Boersma, B.J. & Nieuwstadt, F.T.M. Direct numerical simulation of particle deposition onto a free-slip and to no-slip surface. Physics of Fluids, Vol. 10, 2608-2620 (1998)

Wood, N.B. A simple method for the calculation of turbulent deposition to smooth and rough surfaces. Journal of Aerosol

Science, Vol. 12, No. 3, 275-290 (1981)

Zhang, L. Proc. Of the Sohn Int. Symp. On Advanced Processing of Metals and Materials, Iron and Steel Making, Vol. 2, TMS, Warrendale, PA, p.247 (2006)

Zhao, B. & Wu, J. Modeling particle deposition onto rough walls in ventilation duct. Atmospheric Environment, Vol. 40, 6918-6927 (2006)